Nat. Hazards Earth Syst. Sci. Discuss., 3, 4527–4553, 2015
www.nat-hazards-earth-syst-sci-discuss.net/3/4527/2015/
doi:10.5194/nhessd-3-4527-2015

Natural Hazards and Earth System Sciences
Open Access
Discussions

Liquefaction susceptibility assessment in fluvial plains using high-resolution airborne LiDAR data: the case of the 2012 Emilia earthquake sequence area (Italy)

R. Civico, C. A. Brunori, P. M. De Martini, S. Pucci, F. R. Cinti, and D. Pantosti

Istituto Nazionale di Geofisica e Vulcanologia, Rome, Italy

Received: 15 June 2015 – Accepted: 7 July 2015 – Published: 31 July 2015

Correspondence to: R. Civico (riccardo.civico@ingv.it)

Published by Copernicus Publications on behalf of the European Geosciences Union.

Abstract

We report a case study from the Po River plain region (northern Italy), where a significant liquefaction-related land and property damage occurred during the 2012 Emilia seismic sequence. We took advantage of a 1 m pixel LiDAR Digital Terrain Model (DTM) and of the 2012 Emilia coseismic liquefaction dataset to: (a) perform a detailed geomorphological study of the Po River plain area, (b) quantitatively define the liquefaction susceptibility of the geomorphologic features that experienced different frequency of liquefaction. One main finding is that linear topographic highs of fluvial origin, together with crevasse splays and abandoned riverbeds, acted as preferential location for the occurrence of liquefaction phenomena. Moreover, we quantitatively defined a hierarchy in terms of liquefaction susceptibility for fluvial environments. We observed that a very high liquefaction susceptibility is found in coincidence with fluvial landforms, a high-to-moderate liquefaction susceptibility within a buffer distance of 100 and 200 m from mapped fluvial landforms and a low liquefaction susceptibility outside fluvial landforms and relative buffer areas. LiDAR data allowed a significant improvement in mapping with respect to conventional available topographic data and/or aerial imagery. These results have significant implications for accurate hazard and risk assessment as well as for land-use planning. We propose a potentially simpler approach for liquefaction susceptibility assessment with respect to in situ geotechnical investigations. Our findings can be applied to areas beyond Emilia, characterized by similar fluvial-dominated environments and prone to significant seismic hazard.

1 Introduction

Soil liquefaction is one of the most outstanding hydrogeologic processes that can be originated during earthquakes, provided the existence of saturated loose sandy layers confined by impermeable deposits within a certain distance from the earthquake epicenter. In fact, it is well known that seismic shaking during earthquakes can cause

NHESSD
3, 4527–4553, 2015

water-saturated sediments (low density or uncompacted sandy and/or silty sandy deposits) to temporarily lose strength and to act as a fluid. Because of the peculiar subsurface stratigraphy, this is a common occurrence in alluvial and coastal plains (De Martini et al., 2012).

Liquefaction phenomena are responsible for significant damage to lifelines, infrastructures, agricultural lands and properties, as recently highlighted by the 2010–2011 Canterbury earthquake sequence in New Zealand (van Ballegooy et al., 2014) and by the 2012 Emilia earthquake sequence in the Po Plain, northern Italy (EMERGEO Working Group, 2013). Some of the most massive liquefaction effects worldwide were also induced by the 1964 *M*9.2 Alaska earthquake (Waller, 1966; Seed, 1968) and by the 1964 *M*7.5 Niigata earthquake (Seed and Idriss, 1967), as well as by the 1810–1811 *M*8 New Madrid earthquakes (Obermeier, 1989), the 1995 *M*6.9 Kobe (Japan), the 1999 *M*7.5 Chi-Chi (Taiwan) and the 1999 *M*7.4 Izmit (Turkey) earthquakes (Elgamal et al., 1996; Wang et al., 2003; Wong et al., 2007; Aydan et al., 2008).

The assessment of liquefaction susceptibility in fluvial and coastal plains is a worldwide topic that is growing in interest, probably because of the recent need for "new" areas for urban and industrial development related to the fast growing of global population. The scientific literature clearly highlights the great importance of studies on liquefaction as a contribution to seismic hazard assessment at local and regional scale (for instance the epicentral area of historical or modern earthquakes – Kotoda et al., 1988; Obermeier, 1996). In fact, geotechnical/stratigraphical and geomorphological studies in liquefaction prone areas can provide critical information that will be potentially useful for making accurate hazard and risk maps for land use planning.

Several approaches have been proposed so far in order to predict the liquefaction potential at a site and to compile liquefaction hazard maps. From a geotechnical point of view, the preferred ones are the Liquefaction Potential Index (LPI) and the Liquefaction Severity Number (LSN) (Papathanassiou et al., 2015 and references therein). Both indexes are based on the geotechnical engineering properties of soil

NHESSD
3, 4527–4553, 2015

derived from methods such as Standard Penetration Test (SPT) and Cone Penetration Test (CPT) that require in situ testing. Differently, few studies applied a mainly geomorphological approach for the identification of liquefaction prone regions (among the others: Wakamatsu, 1992; Witter et al., 2006; Ganapathy and Rajawat, 2012; Wotherspoon et al., 2012).

In this paper we report a case study from the Po River plain region (northern Italy), where a significant liquefaction-related land and property damage occurred during the 2012 Emilia seismic sequence. This event highlighted the need for a better understanding of the liquefaction hazard, especially in complex fluvial environments (EMERGEO Working Group, 2013) and references therein).

The huge amount of data on coseismic liquefaction related to the May–June 2012 events (EMERGEO Working Group, 2012a, 2013), offers a unique opportunity to refine our knowledge and methodologies to better understand how the geomorphological setting, besides the stratigraphic and hydrologic conditions, can favor the occurrence of liquefaction phenomena.

Therefore, thanks also to a 1 m pixel airborne LiDAR (Light Detection And Ranging) dataset, we analyzed in detail the correlation between geomorphological features and liquefaction occurrence in the area affected by the 2012 Emilia seismic sequence with the following objectives: (a) perform a detailed geomorphological study of the Po River plain sector that experienced liquefaction phenomena; (b) quantitatively define the areas where liquefaction is more likely to occur in terms of liquefaction susceptibility hierarchy.

Moreover, we introduced a potentially simpler approach for the assessment of liquefaction susceptibility using the liquefaction density (Ld – observed liquefaction effects over a certain area) since it can be calculated entirely by means of remote sensing techniques as opposed to the time-consuming and costly in situ LPI/LNS indexes calculation.

This paper is organized as follows: Sect. 2 describes the geomorphological setting of the epicentral area and provides the background to the 2012 Emilia earthquake

NHESSD
3, 4527–4553, 2015

sequence and the details of the observed liquefaction phenomena; Sect. 3 presents the geomorphological analysis, including landform mapping based on a high-resolution LiDAR Digital Terrain Model (DTM); Sect. 4 presents the results of the quantitative analysis of the spatial distribution of the 2012 coseismic observations. The paper closes with a discussion of the main findings of this work.

2 Study area

2.1 Geomorphological setting

The area struck by the 2012 seismic sequence is characterized by an alluvial plain with flat morphology (average slope less than 3°) and by drainage and fluvial landforms related to the Po, Secchia, Panaro and Reno rivers (Regione Emilia-Romagna, 1999). This landscape has been strongly influenced by human activity since ancient Roman times, by the drainage and reclamation of swamps and marshes, as well as by several diversions of river courses and by the creation of artificial canal and levees.

In more detail, the study area is dominated by a complex drainage and paleo-drainage pattern, characterized by the presence of long and smooth alluvial ridges rising over the floodplain, abandoned riverbeds, levees (both natural and artificial) and crevasse splays. Alluvial ridges are the result of the action of aggrading rivers and are characterized by the rising of the streambed elevation due to deposition of sediments, whereas abandoned riverbeds are the result of a process known as avulsion that is a shift in the main channel bed of the river to a new course. Levees are wedge-shaped ridges of sediment bordering river channels, and generally occur as sinuous, ribbon-like prismatic bodies. They are among the coarser sediments because of their position proximal to the active channel. Crevasse splays form when the levee of the channel is breached and water carrying sediments flows out onto the floodplain depositing sediments in similar pattern to an alluvial fan deposit.

NHESSD
3, 4527–4553, 2015

The general geological-stratigraphic setting of the area is characterized by a subsoil consisting of recent and poorly consolidated fluvial deposits. In more detail, the uppermost tens of meters subsoil is composed by clay, silt and sand deposits organized in layers and lenses, related to the frequent migration of the rivers in the alluvial plain (Regione Emilia-Romagna, 1999; De Martini et al., 2014). Predominantly sandy and silty-sand deposits are generally found in coincidence with river channels, levees and crevasse splays, whereas all the areas dominated by clayey or silty-clayey deposits are related to low-energy environments quite often "trapped" between active- or paleo-riverbeds.

2.2 The 2012 Emilia seismic sequence and observed liquefaction phenomena

In May–June 2012, a seismic sequence struck a broad area of the Emilia-Romagna region in Northern Italy (Fig. 1), resulting in 26 fatalities and hundreds of injured, 15 000 homeless, severe damage of historical centers and industrial areas, and an estimated economic toll of more than 2 billion EUR. The sequence included two mainshocks (M_L 5.9 and M_L 5.8, 20 and 29 May, respectively) and five $M_L \geq 5.1$ events. The whole aftershock area, as defined by more than 1800 $M_L > 1.5$ earthquakes (M_L after Mazza et al., 2012), extended over more than 50 km being elongated in the WNW–ESE direction. The focal mechanisms of the main events consistently show a compressional kinematics with E–W oriented nodal planes (Pondrelli et al., 2012; Scognamiglio et al., 2012; TDMT Database, 2015). These mechanisms are consistent with a horizontal, N–S oriented compression (*P* axes) defined also by present-day stress indicators in the region (Montone et al., 2012 and references therein) and by the GPS-derived velocity field (Devoti et al., 2011).

The 2012 seismic sequence confirmed the Po Plain to be prone to coseismic liquefaction phenomena, as also mentioned in several historical reports of earthquakes occurred in Northern Italy, as the Ferrara 1570, Soncino 1802 and Salò 1901 events (Galli, 2000). The 2012 Emilia earthquake sequence triggered widespread liquefaction through a vast area of the Po River plain (Emilia-Romagna and Lombardia regions).

NHESSD
3, 4527–4553, 2015

An area of approximately 1200 km^2 was covered by the 2012 post-event surveys, and coseismic geological evidences were collected through field reconnaissance and aerial surveys, reports from local people and Web-based surveys (EMERGEO Working Group, 2012a, 2013). More than 1350 coseismic geological effects were identified at the surface (Fig. 1). These consist of liquefaction phenomena induced by seismic shaking (single sand volcano, alignment of sand volcanoes and open fractures created by the sand extrusion – Fig. 2).

Thanks to the information provided by several local eyewitnesses, the EMERGEO personnel in the field and based on the magnitude and timing of the main events, we know that the liquefaction process was induced by the 20 and 29 May mainshocks only. In fact, the only large aftershock that could have produced liquefaction is the 20 May 2012, M_L 5.1, event that occurred only 4 min after the first mainshock, being clearly indistinguishable to eye-witnesses. Moreover, we do have reports of very few (less than 5) liquefaction events occurring at the same site (San Felice sul Panaro municipality, see Fig. 4 in EMERGEO Working Group, 2013) for both 20 and 29 May mainshocks.

Large quantities of ejected sand, silt and water produced damage to commercial buildings, residential houses and infrastructures within the urbanized area. In more detail, subsidence, uplift and lateral spread due to liquefaction of soil at relatively shallow depth were found. Most of the observed damage involved masonry buildings, precast structures, and, in some cases, reinforced concrete buildings. The overall damage to residential buildings was minor but damage was particularly evident for old and poorly maintained masonry structures. On the other hand, significant damage to industrial facilities was observed (Cimellaro et al., 2014).

It was already qualitatively noticed that the presence of subtle fluvial landforms in the area hit by the 2012 seismic sequence strongly influenced and favored the occurrence of liquefactions (Bertolini and Fioroni, 2012; Di Manna et al., 2012; Ninfo et al., 2012; De Martini et al., 2014; EMERGEO Working Group, 2013; Papathanassiou et al., 2012). In fact, looking at the distribution of the liquefaction features, it appears clearly

NHESSD
3, 4527–4553, 2015

that they are not evenly distributed over the area but are mostly arranged in clusters and rectilinear or meander-like alignments (Fig. 3).

Moreover, the maximum distance of the observed liquefaction from the earthquake(s) epicenter is about 30 km. This is in good agreement with national and international empirical relationships available, (Obermeier, 1996; Galli, 2000), between earthquake magnitude and maximum distance for the occurrence of liquefaction phenomena.

3 Methodology

The not homogeneous spatial distribution of the 2012 liquefaction phenomena (see Sect. 2.2) in an area of similar stratigraphy and hydrologic conditions, highlighted the need for understanding better what are the other factors favoring liquefactions. Therefore, we developed a detailed geomorphological characterization of the area, with special focus on subtle landforms of fluvial origin.

We performed a substantial refinement in mapping of the fluvial landforms already identified by Castiglioni et al. (1999), by using a high-resolution (1 m) airborne LiDAR topography, and defined the geomorphologic characteristics of those areas that experienced liquefaction phenomena during the 2012 Emilia seismic sequence.

3.1 High-resolution topography analysis

Widely available digital elevation data (e.g. 10 m Digital Elevation Model – DEM of Italy – Tarquini et al., 2007), are generally too coarse to allow identification and precise mapping of fluvial landforms in alluvial plains (characterized by low morphological gradients). To overcome this drawback, we took advantage of a 1 m pixel resolution LiDAR DTM. The airborne LiDAR survey of the study area was performed in 2008 by Regione Emilia-Romagna using an Optech Gemini ALTM LiDAR Sensor, and covers an area of 693 km^2 (LiDAR accuracy: 0.15 m vertical, 0.35 m horizontal). We processed the original 1 m × 1 m pixel DTM in order to obtain several derivative digital maps

NHESSD
3, 4527–4553, 2015

(shaded relief, slope, aspect, etc.) useful to reveal even the subtlest (0.5 m) topographic features.

In addition, we computed a residual DTM (Residual Relief Surface – RRS – Fig. 4) by removing the regional orographic trend. We eliminated the large-scale variations from the original DTM by calculating a smoothed surface (Grohman and Riccomini, 2009), and we then derived a residual DTM subtracting the smoothed DTM from the original DTM. The residual DTM obtained (RRS) emphasizes the fluvial landforms (both rises and depressions) and make it easier their comparison at different locations, independently from the regional trend. This is clearly visible in Fig. 4, with the RRS showing in a better way depressions and rises over the floodplain and helping substantially the visual interpretation.

3.2 Identification and mapping of fluvial landforms

Our new geomorphological analysis includes the morphogenetic and morphometric landform classification criteria adopted by the previously published 1 : 250 000 geomorphological map of the Po Plain (Castiglioni et al., 1999), but it substantially integrates, and in some cases, deeply revises it. In detail, according to Castiglioni et al. (1999), landforms in the study area are classified as: fluvial and fluvioglacial, aeolian, tectonic and anthropic. We focused our efforts on the precise identification and detailed mapping of selected fluvial landforms either rising over the surrounding floodplain (levee ridges and alluvial ridges, crevasse splays) or incised (traces of abandoned riverbeds).

The map we present comprises an area of 693 km^2 that was surveyed at 1 : 25 000-scale, as the best compromise between the available LiDAR dataset, the desired detail and the time needed to survey the investigated area. We performed mapping mainly based on LiDAR-derived topography and aerial-photo interpretation. We adopted a two-step approach: we first utilized the residual topography to obtain a first-order identification of concavities (depressed landforms) and convexities (rising landforms) in the area, and then we precisely mapped on screen the selected fluvial landforms.

NHESSD
3, 4527–4553, 2015

Figure 5 is an example of the improved identification and mapping of landforms thanks to high-resolution (1 m) LiDAR-derived DTM. Subtle (i.e. less than 1 m relief) features like abandoned riverbeds (Fig. 5b and c) are clearly revealed in the shaded relief image (Fig. 5a and b) as well as by the topographic profile (Fig. 5c).

We mapped in detail more than 100 km^2 of fluvial landforms. The result of our analysis is shown in the map of Fig. 6, together with the observed 2012 liquefaction phenomena (EMERGEO Working Group, 2013).

4 Results

In order to find a simple and homogeneous approach to define areas characterized by different liquefaction potential, we performed a quantitative analysis of the spatial distribution of the 2012 coseismic liquefaction effects using GIS tools. We analyzed the spatial relationships (Overlay and Proximity Analysis) between our precisely-located fluvial landforms and the location of the 2012 liquefaction effects (Fig. 6), identified from both field and aerial surveys, as published by the EMERGEO Working Group (2013). Taking into account the areal extent of the available LiDAR data, we subset from the EMERGEO Working Group (2013) dataset 1306 coseismic effects out of a total of 1350.

As a first consideration, the analysis of the spatial distribution of the liquefaction effects shows that 699 out of a total of 1306 liquefaction phenomena (~ 53 %) are located exactly in coincidence with mapped fluvial landforms. Moreover, alluvial ridges and abandoned fluvial beds were the preferred location for 2012 liquefaction phenomena occurrence (Fig. 7), hosting together ~ 63 % of them, while crevasse splays account for ~ 20 %. As for the remaining liquefaction effects, it should be noted that they are distributed over the floodplain and are not associated with a specific mapped fluvial landform.

Furthermore, in order to homogeneously describe the relationship between 2012 liquefaction phenomena and fluvial landforms, and to find a simple approach for

NHESSD
3, 4527–4553, 2015

the assessment of liquefaction susceptibility to be adopted for future earthquakes, we decided to compute a liquefaction density (Ld) parameter, set as the number of observed coseismic liquefaction effects over a certain area. In general, the whole investigated area (~ 693 km^2) shows an average Ld of 1.9 effects km^2 (1306 effects/693.82 km^2). We then computed the Ld of the mapped fluvial landforms, obtaining a value of 6.6 effects km^2 (699 effects/106.04 km^2), 3.5 times larger than the value computed for the whole area.

Comparing these two values, it is possible to affirm that specific fluvial landforms as abandoned riverbeds, levee ridges and alluvial ridges and crevasse splays are clearly a preferential location for the occurrence of liquefaction vents.

In addition, we set two arbitrary buffer distances from the fluvial landforms (100 and 200 m, respectively) in order to investigate the behavior of the areas located in close proximity of mapped fluvial landforms and thus we computed the relative Ld. A Ld of 2.3 effects km^2 characterizes the buffer distance of 100 m (133 effects/57.62 km^2), whereas a Ld of 1.7 effects km^2 is obtained within a distance of 200 m from fluvial landforms (96 effects/55.96 km^2), these values being 2.9 and 3.9 times smaller than the Ld computed for fluvial features, respectively. Finally, we noticed that, when computed outside the 200 m buffer area, the Ld drops down to a value of 0.8 effects km^2, notably one order of magnitude smaller than the value obtained in coincidence with specific fluvial landforms.

5 Discussion

In this paper, we investigated the correlation between geomorphological features and liquefaction occurrence in the Po River plain that was affected by the 2012 Emilia seismic sequence. In doing this, we took advantage from the huge amount of data on coseismic liquefaction effects related to the 2012 Emilia seismic sequence. Moreover, we put special emphasis on the fluvial features, already recognized as potential control factor for the preferential location of liquefaction phenomena (Bertolini and Fioroni,

NHESSD
3, 4527–4553, 2015

2012; Di Manna et al., 2012; Papathanassiou et al., 2012; EMERGEO Working Group, 2013; De Martini et al., 2014). Ridges, crevasse splays and riverbeds are usually more rich in water-saturated coarse layers with respect to the whole flat alluvial plain (dominated by overflooding un-saturated fine deposits), and for this reason these fluvial features are commonly prone to liquefaction.

We quantitatively defined the liquefaction susceptibility of the geomorphologic features that experienced different frequency of liquefaction using the liquefaction density (Ld). In fact, a hierarchy in terms of liquefaction susceptibility could be set for an ideal fluvial environment by using the ratio between any Ld and the maximum Ld as calculated for the 2012 Emilia case study. We set three classes of susceptibility: very high, high to moderate and low, where the ratio is 1 for very high, between 0.99 and 0.15 for high to moderate, and ≤ 0.15 for low. Figure 8 shows an example of this liquefaction susceptibility assessment from the Sant'Agostino area (southeast of the study area). Here, Lds are: 19.4 for specific fluvial landforms (alluvial and levee ridges, crevasse splays), 16.7 within a buffer distance of 100 m, 8 within a buffer distance of 200 m and 2 outside mapped fluvial landforms and relative buffers. These densities translate to very high susceptibility (ratio 1) for fluvial landforms, high to moderate susceptibility (ratio 0.8 to 0.4) for buffer 100 and 200 m, and low susceptibility (ratio 0.1) outside fluvial features and buffers.

The relation between old and/or former river channels/landforms and liquefaction occurrence was already recognized for some historical and modern earthquakes. Liquefaction-induced damage was observed, among others, during the 1990 Luzon, Philippines earthquake (*M*7.8), the 2007 Niigata–Chuetsu-Oki Japan earthquake (*M*6.8) (Orense et al., 1991, 2008) and the 2010–2011 New Zealand earthquakes (Wotherspoon et al., 2012), showing that coastal and alluvial plains are morphological settings favorable to earthquake induced ground cracks and liquefaction phenomena. Moreover, coastal and alluvial plains are often a preferred location for industrial/power plants and urban centers, thus highlighting the importance of knowing the location

NHESSD
3, 4527–4553, 2015

of old and/or former channels and fluvial landforms when defining liquefaction prone areas.

We present a simpler approach for the assessment of liquefaction susceptibility with respect to traditional geotechnical indexes (LPI or LNS) since it can be calculated entirely by means of remote sensing techniques. In addition, our findings could be useful as a starting point for more detailed investigations based on specific in situ testing.

Finally, we propose to test our findings in future works by comparing to already available LPI/LNS values and to export the same approach in similar fluvial-dominated environment that are prone to significant seismic hazard.

6 Conclusions

On the basis of the analysis of the spatial distribution of the 2012 coseismic observations, one main finding of our study is that linear topographic highs of fluvial origin (alluvial ridges and levees) together with crevasse splays and abandoned riverbeds hosted approximately half (53 %) of the total number of observed liquefaction features, and thus they clearly acted as preferential location for the occurrence of liquefaction phenomena. As for the remaining liquefaction effects, it should be noted that they are distributed over the floodplain and are not associated with a specific mapped fluvial landform. Knowing that alluvial ridges and levees attracted the development of urban settlement and associated infrastructures since ever, and that liquefaction phenomena occurred preferentially within or in proximity of them, the related risk appears to be quite important.

Moreover, we quantitatively defined a hierarchy in terms of liquefaction susceptibility for an ideal fluvial environment by using the 2012 Emilia data. We observed that a very high liquefaction susceptibility is found in coincidence with fluvial landforms, a high to moderate liquefaction susceptibility within a buffer distance of 100 and 200 m from

NHESSD
3, 4527–4553, 2015

fluvial landforms and a low liquefaction susceptibility outside fluvial features and relative buffer areas.

LiDAR data analysis substantially increased the confidence in identifying even subtle (sub-metric) fluvial geomorphic features in areas of very low relief. This resulted in a significant improvement of mapping with respect to conventional available digital topographic data and/or aerial-photo interpretation.

We propose a potentially simpler approach for liquefaction susceptibility assessment with respect to geotechnical calculations that require in situ investigations. These results have significant implications that will be potentially useful for accurate hazard and risk assessment, in order to avoid or mitigate liquefaction-induced damage. Beside the Po River alluvial plain, the findings of this study can be applied to areas beyond Emilia, characterized by similar fluvial-dominated environments and prone to significant seismic hazard.

Author contributions. R. Civico carried out the mapping and the spatial analysis and wrote most of the paper. C. A. Brunori made the LiDAR processing and drafted the manuscript. P. M. De Martini had the idea to analyze the correlation between geomorphological features and liquefaction occurrence and drafted the manuscript. F. R. Cinti, D. Pantosti and S. Pucci provided useful suggestions and much improved the manuscript. All the authors equally contributed to data collection in the field in the framework of the EMERGEO Working Group.

Acknowledgements. The airborne LiDAR survey was kindly released by Regione Emilia-Romagna. We are grateful to Fabio Villani for helpful discussions and advice. The views and conclusions contained in this study are those of the authors and are purely scientific, and they should not be interpreted as necessarily representing official policies, either expressed or implied, of the Istituto Nazionale di Geofisica e Vulcanologia (INGV). The authors and the INGV make no warranty, either expressed or implied, regarding the suitability of these results for a particular use, and they shall not be liable under any circumstances for any direct, indirect, special, incidental, or consequential damages with respect to claims by users of this study.

NHESSD
3, 4527–4553, 2015

References

Aydan, O., Ulusay, R., and Atak, V. O.: Evaluation of ground deformations induced by the 1999 Kocaeli earthquake (Turkey) at selected sites on shorelines, Environ. Geol., 54, 165–182, 2008.

Bertolini, G. and Fioroni, C.: Aerial inventory of surficial geological effects induced by the recent Emilia earthquake (Italy): preliminary report, Ann. Geophys., 55, 705–711, 2012, http://www.ann-geophys.net/55/705/2012/.

Boccaletti, M. and Martelli, L.: Carta sismo-tettonica della Regione Emilia-Romagna scala 1 : 250.000 e note illustrative, S.EL.CA, Firenze, 2004.

Castiglioni, G. B., Biancotti, A., Bondesan, M., Cortemiglia, G. C., Elmi, C., Favero, V., Gasperi, G., Marchetti, G., Orombelli, G., Pellegrini, G. B., and Tellini, C.: Geomorphologic map of the Po Plain, Italy, at a scale of 1 : 250000, Earth Surf. Proc. Land., 24, 1115–1120, 1999.

Cavalli, M., Tarolli, P., Marchi, L., and Fontana, G. D.: The effectiveness of airborne LiDAR data in the recognition of channel-bed morphology, Catena, 73, 249–260, 2008.

Cimellaro, G. P., Chiriatti, M., Roh, H., and Reinhorn, A. M.: Seismic performance of industrial sheds and liquefaction effects during May 2012 Emilia earthquakes sequence in northern Italy, J. Earthq. Tsunami, 8, 23, doi:10.1142/S1793431114500092, 2014.

De Martini, P. M., Cinti, F. R., Cucci, L., Smedile, A., Pinzi, S., Brunori, C. A., and Molisso, F.: Sand volcanoes induced by the 6 April 2009 Mw 6.3 L'Aquila earthquake: a case study from the Fossa area, Italian, J. Geosci., 131, 410–422, 2012.

De Martini, P. M., Alfonsi, L., Brunori, C. A., Campagnoli, P., Cinti, F. R., Civico, R., Cucci, L., Gambillara, R., Livio, F., Michetti, A. M., Molisso, F., Pantosti, D., Pinzi, S., Pucci, S., and Venuti, A.: Geological and geophysical approaches for the definition of the areas prone to liquefaction and for the identification and characterization of paloeliquefaction phenomena, the case of the 2012 Emilia epicentral area, Italy, in: Engeneering Geology for Society and Territory, Vol. 5, Chapter 184, edited by: Lollino, G. et al., Springer International Publishing, Switzerland, doi:10.1007/978-3-319-09048-1_184, 2014.

Devoti, R., Esposito, A., Pietrantonio, G., Pisani, A. R., and Riguzzi, F.: Evidence of large scale deformation patterns from GPS data in the Italian subduction boundary, Earth Planet. Sc. Lett., 311, 230–241, 2011.

NHESSD
3, 4527–4553, 2015

Di Manna, P., Guerrieri, L., Piccardi, L., Vittori, E., Castaldini, D., Berlusconi, A., Bonadeo, L., Comerci, V., Ferrario, F., and Gambillara, R.: Ground effects induced by the 2012 seismic sequence in Emilia: implications for seismic hazard assessment in the Po plain, Ann. Geophys., 55, 697–703, 2012, http://www.ann-geophys.net/55/697/2012/.

Elgamal, A. W., Zeghal, M., and Parra, E.: Liquefaction of reclaimed island in Kobe, Japan, J. Geotech. Eng-ASCE, 122, 39–49, 1996.

EMERGEO Working Group: Technologies and new approaches used by the INGV Emergeo working group for real-time data sourcing and processing during the Emilia-Romagna (northern Italy) 2012 earthquake sequence, Ann. Geophys., 55, 689–695, 2012a, http://www.ann-geophys.net/55/689/2012/.

EMERGEO Working Group: A Photographic Dataset of the Coseismic Geological Effects Induced on the Environment by the 2012 Emilia (Northern Italy) Earthquake Sequence, Miscellanea INGV, 16, ISSN 2039–6651, available at: http://www.earth-prints.org/handle/2122/8455, last accessed: 27 February 2015, 2012b.

Emergeo Working Group: Liquefaction phenomena associated with the Emilia earthquake sequence of May–June 2012 (Northern Italy), Nat. Hazards Earth Syst. Sci., 13, 935–947, doi:10.5194/nhess-13-935-2013, 2013.

Galli, P.: New empirical relationships between magnitude and distance for liquefaction, Tectonophysics, 324, 169–187, 2000.

Ganapathy, G. P. and Rajawat, A. S.: Evaluation of liquefaction potential hazard of Chennai City, India: using geological and geomorphological characteristics, Nat. Hazards, 64, 1717–1729, 2012.

Grohmann, C. H. and Riccomini, C.: Comparison of roving-window and search-window techniques for characterising landscape morphometry, Comput. Geosci., 35, 2164–2169, doi:10.1016/j.cageo.2008.12.014, 2009.

Kotoda, K., Wakamatsu, K., and Masahiko, O.: Mapping liquefaction potential based on geomorphological land classification, in: Proceedings of Ninth World Conference on Earthquake Engineering, Tokyo, Japan, 2–9 August 1988, III, 195–200, 1988.

Mazza, S., Basili, A., Bono, A., Lauciani, V., Mandiello, A. G., Marcocci, C., and Selvaggi, G.: AIDA – seismic data acquisition, processing, storage and distribution at the National Earthquake Center, INGV, Ann. Geophys., Ann. Geophys., 55, 8 pp., doi:10.4401/ag-6145, 2012.

NHESSD
3, 4527–4553, 2015

Montone, P., Mariucci, M. T., and Pierdominici, S.: The Italian present-day stress map, Geophys. J. Int., 189, 705–716, 2012.
Ninfo, A., Zizioli, D., Meisina, C., Castaldini, D., Zucca, F., Luzi, L., and De Amicis, M.: The survey and mapping of sand-boil landforms related to the Emilia 2012 earthquakes: preliminary results, Ann. Geophys., 55, 727–733, 2012, http://www.ann-geophys.net/55/727/2012/.
Obermeir, S. F.: The new Madrid earthquakes: an engineering-geologic interpretation of relic liquefaction features, U.S. Geol. Surv. Prof. Pap., 1336-B, 114, United States Government Printing Office, Washington, USA, 1989.
Obermeier, S. F.: Use of liquefaction-induced features for paleoseismic analysis – an overview of how seismic liquefaction features can be distinguished from other features and how their regional distribution and properties of source sediment can be used to infer the location and strength of Holocene paleo-earthquakes, Eng. Geol., 44, 1–76, 1996.
Orense, R. P., Towhata, I., and Ishihara, K.: Soil liquefaction in Dagupan City during the 1990 Luzon, Philippines earthquake, in: Proc. 26th Nat. Conf. on Soil Mech. and Found. Eng., JSSMFE, 871–874, 1991.
Orense, R. P., Hyodo, M., Kanda, H., and Ohashi, J.: Geotechnical aspects of the 2007 Niigataken Chuetsu-Oki, Bulletin of the New Zealand Society for Earthquake Engineering, 41, 83–89, 2008.
Papathanassiou, G., Caputo, R., and Rapti-Caputo, D.: Liquefaction phenomena along the palaeo-Reno River caused by the 20 May 2012 Emilia (northern Italy) earthquake, Ann. Geophys., 55, 735–742, 2012, http://www.ann-geophys.net/55/735/2012/.
Papathanassiou, G., Mantovani, A., Tarabusi, G., Rapti, D., and Caputo, R.: Assessment of liquefaction potential for two liquefaction prone areas considering the 20 May 2012 Emilia (Italy) earthquake, Eng. Geol., 189, 1–16, 2015.
Pondrelli, S., Salimbeni, S., Perfetti, P., and Danecek, P.: Quick regional centroid moment tensor solutions for the Emilia 2012 (northern Italy) seismic sequence, Ann. Geophys., 55, 615–621, 2012, http://www.ann-geophys.net/55/615/2012/.
Regione Emilia-Romagna: Carta Geologica di pianura dell'Emilia-Romagna alla scala 1 : 250.000, D. Preti. S.EL.CA, Firenze, 1999.

NHESSD
3, 4527–4553, 2015

Scognamiglio, L., Margheriti, L., Mele, F. M., Tinti, E., Bono, A., De Gori, P., Lauciani, V., Lucente, F. P., Mandiello, A. G., and Marcocci, C.: The 2012 Pianura Padana Emiliana seimic sequence: locations, moment tensors and magnitudes, Ann. Geophys., 55, 549–559, 2012, http://www.ann-geophys.net/55/549/2012/.

Seed, H. B.: Landslides during earthquakes due to soil liquefaction, Journal of the Soil Mechanics and Foundations Division, 94, 1055–1122, 1968.

Seed, H. B. and Idriss, I. M.: Analysis of soil liquefaction: Niigata earthquake, Journal of the Soil Mechanics and Foundations Division, 93, 83–108, 1967.

Tarquini, S., Isola, I., Favalli, M., Mazzarini, F., Bisson, M., Pareschi, M. T., and Boschi, E.: Tinitaly/01: a new triangular irregular network of Italy, Ann Geophys., 50, 407–425, 2007.

TDMT Database: Real-time determination of seismic moment tensor for the Italian region, INGV, available at: http://cnt.rm.ingv.it/en/tdmt (last access: 19 February 2015), 2015.

van Ballegooy, S., Malan, P., Lacrosse, V., Jacka, M. E., Cubrinovski, M., Bray, J. D., O'Rourke, T. D., Crawford, S. A., and Cowan, H.: Assessment of liquefaction-induced land damage for residential Christchurch, Earthq. Spectra, 30, 31–55, 2014.

Wakamatsu, K.: Evaluation of liquefaction susceptibility based on detailed geomorphological classification, in: Proceedings of Technical Papers of Annual Meeting Architectural Institute of Japan, B, 1443–1444, 1992.

Waller, R. M.: Effects of the March 1964 Alaska earthquake on the hydrology of south central Alaska, U.S. Geol. Surv. Prof. Pap., 544-A, United States Government Printing Office, Washington, USA, 1966.

Wang, C. Y., Dreger, D. S., Wang, C. H., Mayeri, D., and Berryman, J. G.: Field relations among coseismic ground motion, water level change and liquefaction for the 1999 Chi-Chi (mw = 7.5) earthquake, Taiwan, Geophys. Res. Lett., 30, 1890, doi:10.1029/2003GL017601, 2003.

Witter, C. R., Knudsen, L. K., Sowers, M. J., Wentworth, M. C., Koehler, D. R., and Randolph, C. E.: Maps of Quaternary Deposits and Liquefaction Susceptibility in the Central San Francisco Bay Region, California, U.S. Geological Survey Open-File Report 2006-1037, 43 pp., 2006.

Wong, A. and Wang, C. Y.: Field relations between the spectral composition of ground motion and hydrological effects during the 1999 Chi-Chi (Taiwan) earthquake, J. Geophys. Res., 112, B10305, doi:10.1029/2006JB004516, 2007.

NHESSD
3, 4527–4553, 2015

Wotherspoon, L. M., Pender, M. J., and Orense, R. P.: Relationship between observed liquefaction at Kaiapoi following the 2010 Darfield earthquake and former channels of the Waimakariri river, Eng. Geol., 125, 45–55, 2012.

NHESSD
3, 4527–4553, 2015

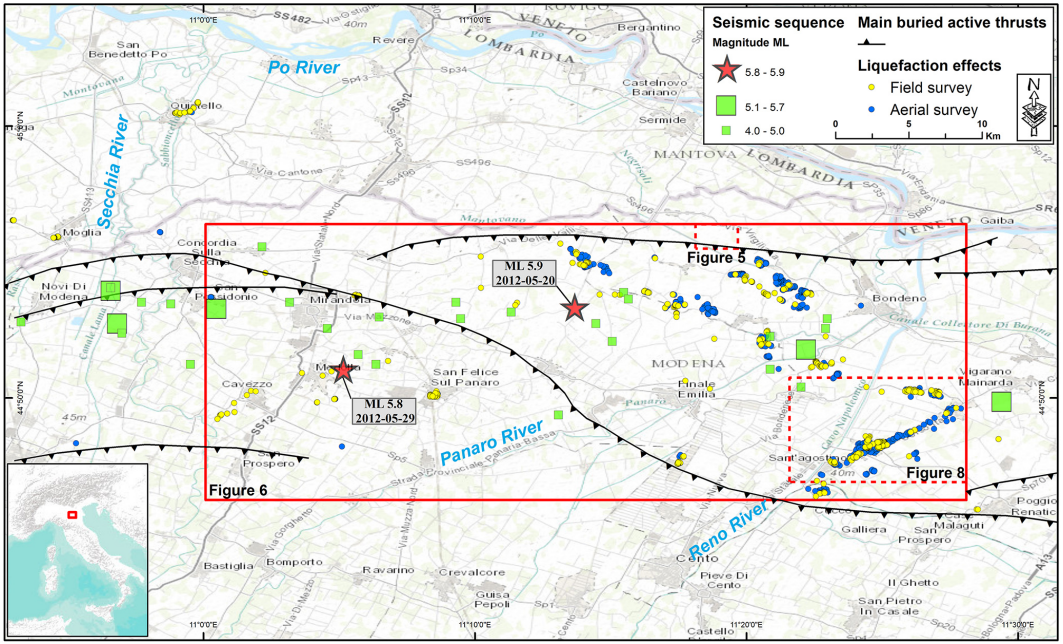

Figure 1. Area of the 2012 Emilia earthquake sequence: red stars locate mainshocks; large green squares locate five $M \geq 5.1$ eqs, small green squares locate M 4.0 < x < 5.0 eqs; main buried thrusts from Boccaletti and Martelli (2008); red rectangles locate Figs. 5, 6 and 8, respectively. Liquefaction effects recognized from field (yellow dots) and aerial (blue dots) surveys are reported.

NHESSD
3, 4527–4553, 2015

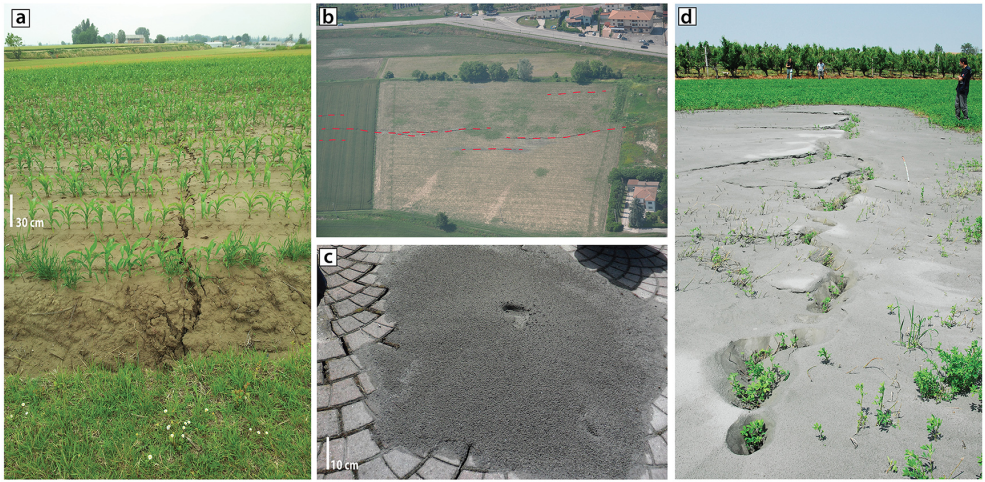

Figure 2. Examples of observed liquefaction phenomena produced by the 2012 Emilia seismic sequence: (**a** and **b**) fractures; **(c)** single sand volcano; **(d)** alignment of sand volcanoes (photos courtesy of EMERGEO Working Group, 2012b).

NHESSD
3, 4527–4553, 2015

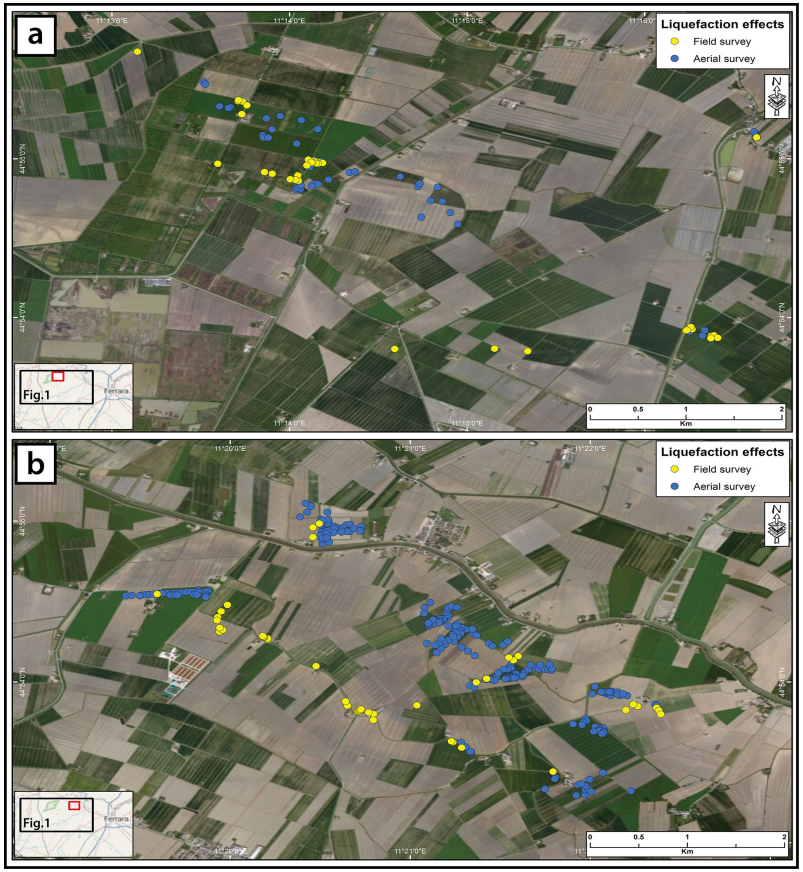

Figure 3. Subset of the 2012 Emilia sequence liquefaction effects (from both field and aerial surveys) showing their arrangement in clusters and rectilinear or meander-like alignments.

NHESSD
3, 4527–4553, 2015

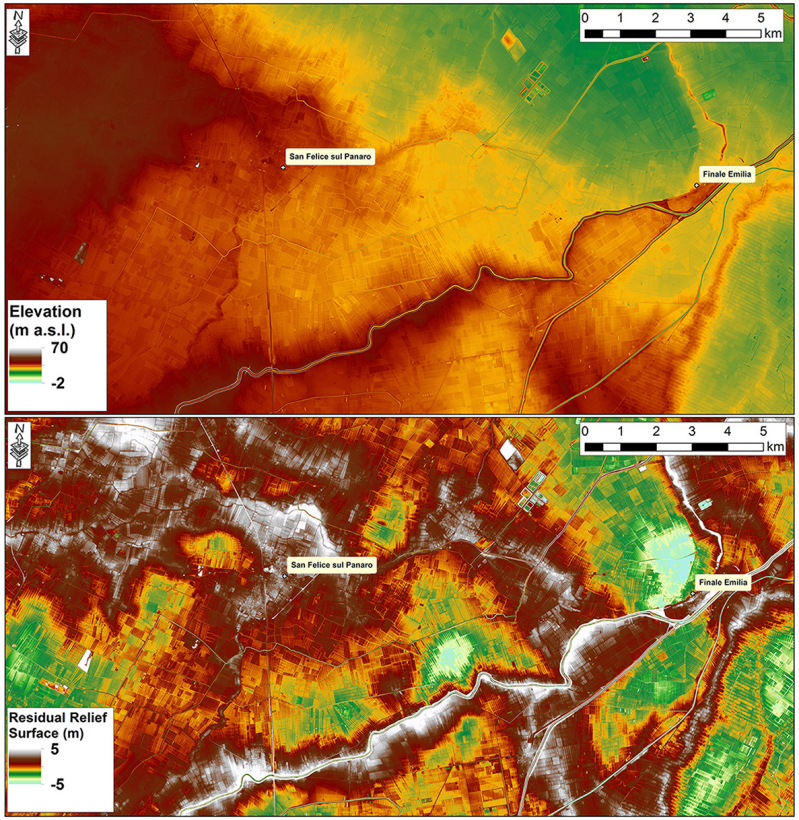

Figure 4. Comparison between the original 1 m pixel LiDAR DTM (upper panel) and the Residual Relief Surface (RRS – lower panel). The calculation of the RRS emphasizes rising and depressed landforms and makes easier their comparison at different locations, independently from the regional trend of the topography.

NHESSD
3, 4527–4553, 2015

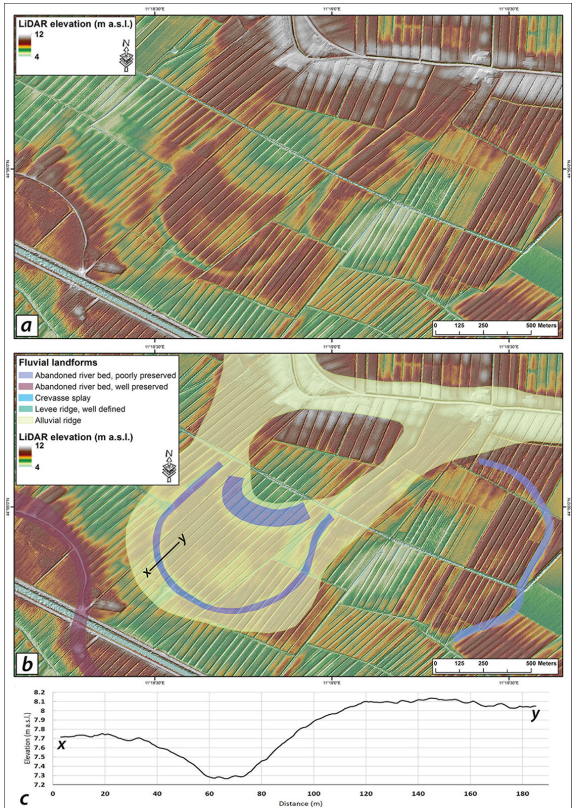

Figure 5. Example of improved high-resolution LiDAR-derived digital elevation model and application in geomorphological mapping from an area north of Gavello (FE), northern portion of the study area (see Fig. 1 for location): **(a)** 1 m pixel LiDAR DTM with no interpretation; **(b)** same area showing subtle fluvial landforms like alluvial ridges and abandoned riverbeds; **(c)** topographic profile (black line in Fig. 5b) showing the subtle morphologic expression (total relief less than 1 m) of the abandoned riverbed.

NHESSD
3, 4527–4553, 2015

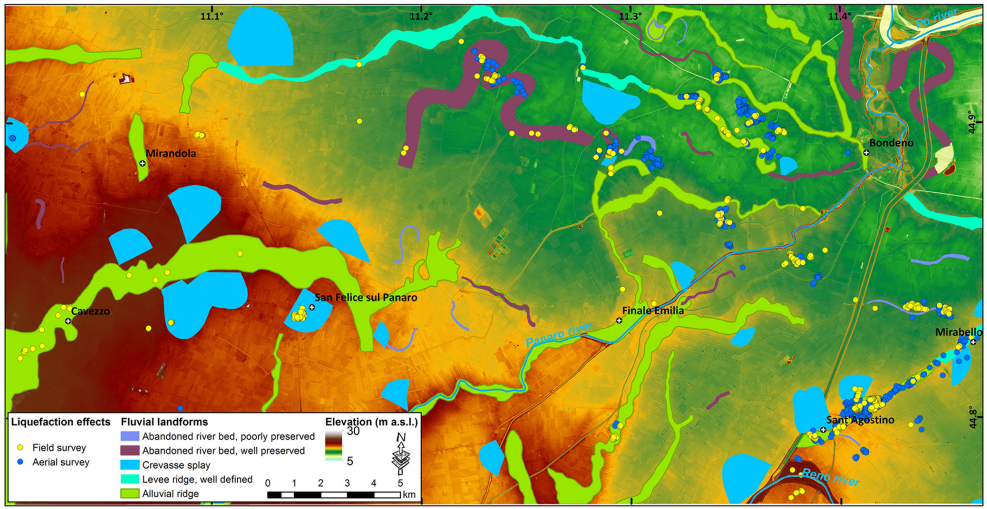

Figure 6. Geomorphological map of the study area (see Fig. 1 for location) showing selected fluvial landforms and observed liquefaction phenomena.

NHESSD
3, 4527–4553, 2015

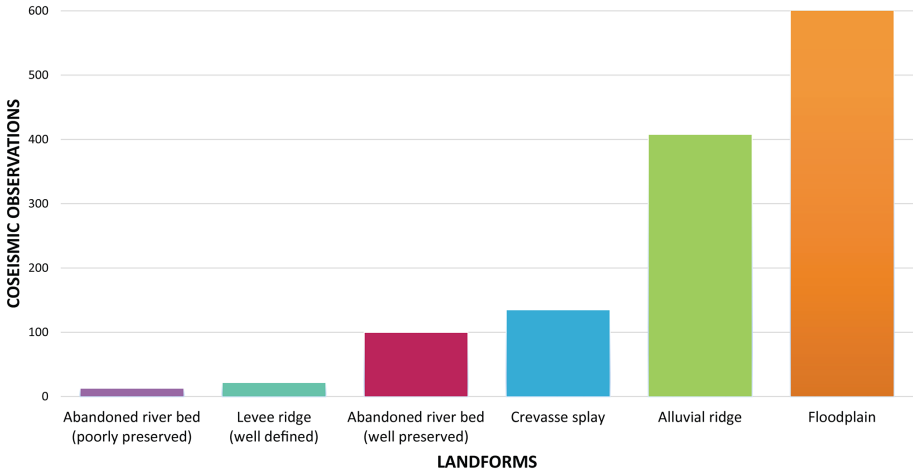

Figure 7. Distribution of the observed coseismic liquefaction effects with respect to mapped fluvial landforms (see Fig. 6).

NHESSD
3, 4527–4553, 2015

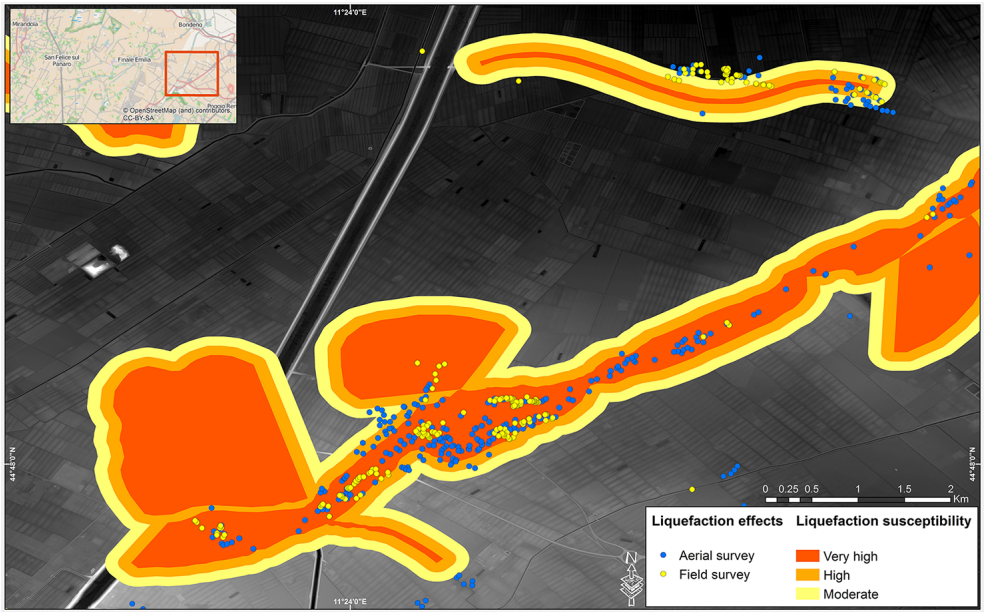

Figure 8. Liquefaction susceptibility hierarchy map for the Sant'Agostino village area (see Fig. 1 for location).

NHESSD
3, 4527–4553, 2015